International Journal of Refrigeration 145 (2023) 158–167

Contents lists available at ScienceDirect

International Journal of Refrigeration

journal homepage: www.elsevier.com/locate/ijrefrig

Refrigerant charge distribution in brine-to-water heat pump using R290 as refrigerant

Distribution de la charge en frigorigène dans une pompe à chaleur saumure/eau utilisant le R290 comme frigorigène

Luis Sánchez-Moreno-Giner [a,b,*], Timo Methler [b], Francisco Barceló-Ruescas [a], José Gonzálvez-Maciá [a]

[a] *Instituto Universitario de Investigación de Ingeniería Energética. Universitat Politècnica de València, Camino de Vera s/n, 46022 Valencia, Spain*
[b] *Fraunhofer-Institut für Solare Energiesysteme ISE, Heidenhofstr. 2, D-79110, Germany*

ARTICLE INFO

Keywords:
R290
Low refrigerant charge
Refrigerant distribution
Brine-to-water heat pump
Mots clés:
Frigorigènes naturels
Faible charge en frigorigène
Distribution du frigorigène
Décarbonation
Pompe à chaleur saumure-eau

ABSTRACT

This paper presents experimental results from a brine-to-water heat pump used for space heating at low temperature, with a low refrigerant charge of R290 (propane). Performance and refrigerant distribution were analysed in every test condition studied. Performance results show a declared heating capacity of 9.5 kW, obtaining a specific capacity (C_c) of 48.7 kW rmkg^{-1} and a seasonal coefficient of performance of 4.01. In terms of refrigerant distribution, at the nominal point, 41.5% of the refrigerant is located in the compressor, mainly dissolved in the oil, and the rest is separated almost evenly in both heat exchangers, 23.9% in the condenser and 27.8% in the evaporator; having the lines and accessories (pneumatic-ball valves) the remaining 6.8%. Due to this fact, reducing oil solubility by heating the crankcase or increasing the superheat (SH) has a positive impact on the refrigerant charge reduction, but it also affects the coefficient of performance.

1. Introduction

In 2019, in Europe, energy consumption in households accounted for 26.3% of the total energy consumed. In these buildings, heating, cooling, and domestic hot water (DHW) production correspond to 78.4% of the total energy consumed, and 75% of heating and domestic hot water in European buildings is produced using fossil fuels ("Energy consumption in households - Statistics Explained," 2021). To achieve the objective of being climate-neutral by 2050 (European Commission, 2019), there shall be a progressive substitution of gas boilers with a more sustainable alternative, such as biomass boilers or heat pumps. Nevertheless, some improvements in vapour compression cycles for domestic applications must be made to comply with European refrigerant regulations.

There have been European regulations concerning refrigerant emissions contributing to the greenhouse effect. Currently, the European Union restricts the commercially available amount of Hydrofluorocarbons (HFCs), which are the primary refrigerants used for domestic applications. The amount presently allowed is half the amount commercialised yearly from 2009 to 2012 (Regulation (EU) No 517/2014, 2014). Consequently, there must be a reduction of HFCs employed in domestic heating applications. Potential solutions are reducing the amount of refrigerant charge or replacing it with refrigerants with less global warming potential (GWP). The current trend is to change the refrigerant used with natural refrigerants such as carbon dioxide, ammonia, or hydrocarbons(Domanski et al., 2017; Lorentzen, 1995; McLinden et al., 2017; Pitarch et al., 2017) or synthetic HFOs (Kujak and Schultz, 2016). All these alternatives (except carbon dioxide) have flammability or toxicity problems. For this reason, refrigerant charge reduction has become an important matter lately, due to the impact on the overall carbon footprint and the hazard potential due to flammability or toxicity.

The current limitation for hydrocarbons without extra security measures is 150 g of refrigerant (European Committee for Standardization, 2016). Because of this limit, a new indicator is proposed to

* Corresponding author.
E-mail address: luis.sanchez@iie.upv.es (L. Sánchez-Moreno-Giner).

https://doi.org/10.1016/j.ijrefrig.2022.10.013
Received 4 May 2022; Received in revised form 12 October 2022; Accepted 15 October 2022
Available online 19 October 2022
0140-7007/© 2022 The Authors. Published by Elsevier B.V. This is an open access article under the CC BY-NC-ND license (http://creativecommons.org/licenses/by-nc-nd/4.0/).

Nomenclature

b	Systematic standard uncertainty
C_c	Charge specific capacity, kW kg^{-1}
c_p	Specific Heat, J kg^{-1} K^{-1}
$\dot{m}$	Mass flow rate, kg s^{-1}
n	Compressor rotational speed, s^{-1}
P	Pressure, Pa
$\dot{Q}$	Thermal capacity, W
rps	Revolutions per second
s	Random standard uncertainty
T	Temperature, °C
u	Overall standard uncertainty
U_i	Overall uncertainty at i% confidence level
V	Volume, m^3

Greek symbols

δ	Temperature approach
Δ	Temperature difference

Subscripts

b	Brine
comp	Compressor
cond	Condenser
ext	Extracted
evap	Evaporator
ext	Extracted
h	Heating
i	Section. i = 1: Compressor; i = 2: Condenser; i = 3: Evaporator
in	Inlet
ins	Inserted
N	Nitrogen
Oil	Compressor's oil
out	Outlet
rem	Remaining
suc	Suction
w	Water

Abbreviations

3WV	Three-way valve
BPHE	Brazed Plates Heat Exchanger
COP	Coefficient of Performance
CP	Circulation pump
DHW	Domestic hot water
EEV	Electronic expansion valve
GWP	Global Warming Potential
HFC	Hydrofluorocarbon
MV	Manual Valve
SCOP	Seasonal coefficient of performance
Sc	Subcooling
Sh	Superheat
QCV	Quick-closing valve

evaluate and compare the systems and determine how refrigerant demanding is. This indicator is the specific charge, calculated as refrigerant charge divided by useful capacity (cooling or heating), in kg kW^{-1}, or the inverse figure, the charge specific capacity (C_c) in kW kg^{-1} (Clodic and Palandre, 2002; Marvillet, 1995).

Poggi et al. (2008) presented an overview of the charge specific capacity regarding the application of refrigeration systems. The maximum C_c calculated in this overview are: 20 kW kg^{-1} for air conditioning, 3 kW kg^{-1} for domestic refrigeration, 7 kW kg^{-1} for commercial refrigeration, and 2 kW kg^{-1} for industrial refrigeration.

Concerning refrigeration systems, Hrnjak and Litch (2008) presented in their work an air-cooled chiller using ammonia as refrigerant with a C_c of 55 kW kg^{-1}. In domestic air conditioning systems, Mulroy and Didion (1985); Xu et al. (2016) and (Chen et al., 2019) presented works about refrigerant distribution with C_c values of 2.3 kW kg^{-1}, 16.6 kW kg^{-1}, and 8.5 kW kg^{-1}, respectively, using the first R22 and the others R290. In automotive air conditioning, in the works of Hrnjak and Hoehne (2004); Li and Hrnjak (2015) and Peuker (2010) C_c of 10.8 kW kg^{-1} (R290), 12 kW kg^{-1} (R290), and 4.15 kW kg^{-1} (R134a), are respectively presented.

In heat pump systems, there are also some works related to charge minimisation from which the C_c (heating capacity in this case) can be extracted. Fernando et al. (2004), in their work, presented a brine-to-water heat pump working with 200 g of R290 which in the condition B-2W40[1] obtained a C_c of 25 kW kg^{-1}. Also, Corberán et al. (2008) presented a water-water heat pump using 550 g of R290, reporting a C_c of 25.5 kW kg^{-1} at W10W45 and Sieres et al. (2020) proposed a brine-to-water with DHW production using R407C with a value of 8 kW kg^{-1} at B10W35. Lastly, Andersson et al. (2018) presented a ground source heat pump using R290 and reached a C_c of 94 kW kg^{-1} with an automotive compressor and non-commercial heat exchangers.

The problem with the charge specific capacity is that it depends on the application and the condition studied, which is complex and unreliable to extrapolate, even more when extrapolating from cooling to heating or vice versa. Regarding heat pumps, only one work (Andersson et al., 2018) has been obtained enough heating capacity able to cover the domestic heating range (typically 12 kW (Lund, 2001)), but this work was performed different working conditions than established in the measurement standards, and the unit was built with prototype brazed plates heat exchangers (BPHEs) and an automotive compressor.

Last decade, new compressors using specific oil suitable for propane and asymmetric BPHEs using narrower channels for the refrigerant side were introduced in the heat pump market sector resulting in higher values of charge specific capacity but there are no reported results of performance and charge distribution with these new technologies.

Based on the presented issues, the objectives of this research are:

(i) To study the performance of a brine-to-water heat pump working with propane as refrigerant for domestic applications at different working conditions using the last generation components available in the market.
(ii) To analyse the refrigerant charge distribution in the different components of the heat pump in order to identify further improvements in charge reduction for these types of units.

For this reason, the experimental performance results and refrigerant distribution are presented through the components of a brine-to-water heat pump. Firstly, there is a definition of the prototype, the sensors employed, and the tests performed. Afterwards, the performance and charge distribution results are presented to see the possibility of having enough capacity for domestic heating with only 150 g of propane and strategies to reduce the amount required without compromising performance.

[1] first letter is the source type, first number is the source temperature, second letter is the sink type, second number is the sink temperature. Source/sink types are B: brine, W:Water, A:Air

2. Methodology

In this work, the prototype employed is a brine-to-water heat pump with a design heating capacity of 9.5 kW for the nominal operating point of source at 0°C and sink at 35°C with an approximate refrigerant charge of 195 g of R290 to achieve proper performance.

The prototype is a non-reversible brine-to-water heat pump with two brazed plates heat exchangers as condenser and evaporator. Table 1 lists the elements of the heat pump.

The test bench has two secondary loops (sink to water and source from ethylene glycol-water brine 40% in volume) able to control the temperature and mass flow to the condition set according to the standard EN14511–3 (European Committee for Standardization 2019a).

Fig. 1 shows the scheme of the components regarding the heat pump and the control system. In the scheme, there are three main parts differentiated, the refrigerant side, the loop able to control secondary fluid in the condenser and the loop able to control the secondary fluid in the evaporator.

On the refrigerant side, it is shown the elements mentioned before (compressor, condenser, electronic expansion valve and evaporator), the quick closing valves (QCV) and sensors measuring main temperatures and pressures of the refrigerant circuit.

A variable circulation pump drives water on the sink side, and its mass flow rate is measured with a Coriolis mass flow meter. The water flow rate is adjusted according to the test requirements. The water inlet temperature is controlled by a three-way valve ($3WV_1$), dissipating more or less heat to the sink side. On the secondary side of the evaporator, the fluid is a mixture of ethylene glycol (40% in volume) and water (60%). The control loop is similar to the sink side, $3WV_2$ controls the inlet brine temperature, and the frequency of the circulation pump is adjusted to set the required value by the test.

The temperature sensors used in the refrigerant circuit are PT100 class B, located in contact with the pipe with thermal paste, except for the measure of outlet temperature of the condenser, which has been measured in the stream of the refrigerant flow. Pressure in the refrigerant circuit is measured with pressure transducers type 1 from Table 2. For the water and brine temperature, it has been used PT100 class A in the stream.

For the refrigerant extraction and weight, it has been used additional sensors. Scale 1 measures the cylinder weight permanently connected to the unit to measure the refrigerant amount extracted. Scale 2 measures the cylinder weight used to charge the unit. Additional pressure transducers (pressure transducer 2 in the table) were used to measure the gas pressure in the section after extraction.

Table 2 shows the sensors used in the characterisation tests and their associated fixed uncertainty. Systematic uncertainty in the RTDs is taken from the standard (IEC, 2022) and for the rest of the sensors by the information given by the manufacturer.

2.1. Test procedure

Each test performed has two steps: performance and refrigerant charge distribution.

The unit is charged from pure propane cylinder (not recovered), and the charge inserted (m_{ins}) is measured with scale 2 (see Table 2). The initial tare of the refrigerant cylinder is 7.7 kg.

After the heat pump is charged, it is switched on, and the control loops are set to maintain the objective values of $T_{w,in}, \Delta T_w, T_{b,in}, \Delta T_b$ required by the test. After reaching stability, when inlet water and brine mean temperatures differences to the objective do not exceed $\pm 0.2\ K$ and individual values differences to the mean do not exceed $\pm 0.5\ K$ and outlet water and brine mean temperatures differences to the objective do not exceed $\pm 0.3\ K$ and individual differences to the mean do not exceed $\pm 0.6\ K$ (European Committee for Standardization, 2019a), data is recorded to at least 30 min.

At this point, heating capacity and coefficient of performance (COP) are calculated with the data recorded during the stability period as:

$$\dot{Q}_h = \dot{m}_w c_p \left(T_{w,out} - T_{w,in}\right) \tag{1}$$

$$COP = \frac{\dot{Q}_h}{\dot{E}} \tag{2}$$

The refrigeration charge distribution step is started afterwards. Quick closing valves actuate (closing sections in less than 1 s), isolating the different sections of the heat pump and the compressor stops by the trigger of high and low-pressure switches.

Then, charge extraction is performed with the sample cylinder shown in Fig. 2.

The sample cylinder is cooled down with liquid nitrogen after weighting the tare weight (m_1). Then the manual valve 1 (MV_1) is opened, starting the refrigerant collection inside the sample cylinder until the equilibrium is reached. Lastly, the liquid nitrogen is evaporated, and the moist and ice are removed from the walls using an infrared heater, then the system is weighted (m_2). The refrigerant extracted is the subtraction of the tare weight (m_1) from the last value (m_2) as:

$$m_{ext,i} = m_2 - m_1 \tag{3}$$

The remaining refrigerant in the section ($m_{st,i}$) is at very low pressure (~1 kPa) in vapour state. This remaining charge is estimated with vapour density calculated from measurement of pressure (location 107) and temperature (location 108), and the section volume V_i.

The section volume was measured before with an isothermal gas test using gaseous nitrogen. In each section, nitrogen charge (m_N) was measured, and nitrogen density can be calculated with the measurements of pressure and temperature using Refprop Database Version 10 (Lemmon et al., 2018). Volume in each section is the result of (4):

$$V_i = \frac{m_{N,i}}{\rho_i} \tag{4}$$

Calculated volume in each section and comparison with hand calculations from components characteristics are shown in Table 3 (except from Section 1, where there is no internal volume data available from the compressor). Comparison agreed in order of magnitude with calculated estimations.

After all the sections are extracted, all the QCV are opened to extract the refrigerant that was inside the ball mechanism of the valves (m_{QCV}).

Then, the total mass extracted in the heat pump is:

$$m_{ext} = \sum \left(m_{ext,i} + m_{rem,i}\right) + m_{QCV} \tag{5}$$

And this extracted and inserted mass is compared with its associated uncertainties:

$$m_{ext} \pm U_{95} = m_{ins} \pm U_{95} \tag{6}$$

If measurements do not comply with this equality, the test is rejected.

2.2. Uncertainty analysis

Table 4 shows each variable's systematic, random, and overall uncertainty in the nominal test (B0W35 at 60 rps). Systematic uncertainty was extracted from catalogue data (Table 2). Only m_{ins} was measured as a single point, all the other values are recorded every second. This fact

Table 1
Elements of the heat pump.

Element	Model	Type	Specifications CC/Internal volume	Number of plates
Compressor	TPB306	Rotary	30.6 cm^3	–
Condenser	CB24	Asymmetric	0.39 dm^3	38
Evaporator	CB65	Symmetric	0.66 dm^3	16

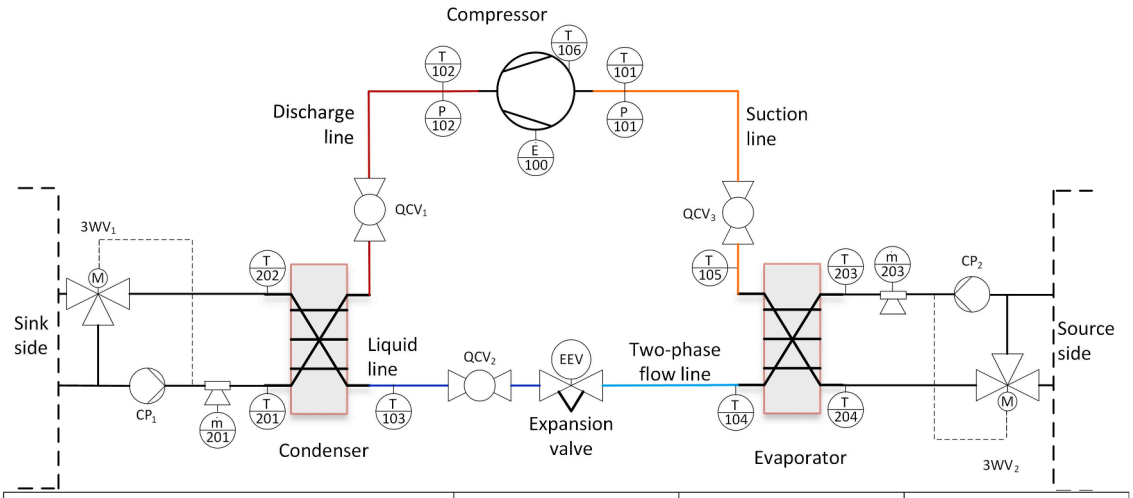

Temperature				Pressure		Mass flow rate		Power absorbed	
Refrigerant side		Secondary fluid side		Refrigerant side		Secondary fluid side			
Location	Variable	Location	Variable	Location	Variable	Location	Variable	Location	Variable
101	$T_{comp,in}$	201	$T_{w,in}$	101	P_{suc}	201	$\dot{m}_w$	100	$\dot{E}_{comp}$
102	$T_{comp,out}$	202	$T_{w,out}$	102	P_{dis}	203	$\dot{m}_b$		
103	$T_{cond,out}$	203	$T_{b,in}$						
104	$T_{evap,in}$	204	$T_{b,out}$						
105	$T_{evap,out}$								
106	T_{oil}								

Fig. 1. Test bench scheme.

Table 2
Sensors employed and uncertainty.

Variable measured	Type of sensor	Systematic uncertainty 2σ (95% Confidence)
Temperature	PT100 class B	±0.3 + 0.005T (°C)
Temperature	PT100 class A	±0.07 (°C)
Temperature	Thermocouple type T	±0.8 (°C)
Circuit Pressure	Pressure transducer 1	0.25% of the span
Gas pressure	Pressure transducer 2	0.04% of the span
Mass flow	Coriolis mass flow meter	0.10% of the measure
Mass extracted	Scale 1	0.01+0.002 m (g)
Mass inserted	Scale 2	0.2 (g)
Power absorbed	Power analyser	0.6% of the span

explains the difference in the random error of the m_{ins} and m_{ext} and explains why the random error of some of these variables is negligible.

Overall uncertainty is calculated from the combined standard uncertainty using the assumption of large-sample uncertainty (Coleman et al., 2009; International Organization for Standardization (ISO), 1995; Joint Committee for Guides in Metrology (JCGM), 2008) as:

$$U_{95} = 2u = 2\sqrt{s^2 + b^2} \tag{7}$$

Uncertainty of heating capacity $\dot{Q}_h$, COP and remaining mass in the components m_{rem} is calculated using the Taylor Series Method for the propagation of uncertainties:

$$U_{95} = \sqrt{\sum_{i=1}^{N}\left(\frac{\partial f}{\partial x_i}\right)U_i^2} \tag{8}$$

Where f is a function of the measured variables x_i.

Taking the nominal point as a reference, in the performance results, the propagation of uncertainty of $\dot{Q}_h$ and COP results in ±54 W and

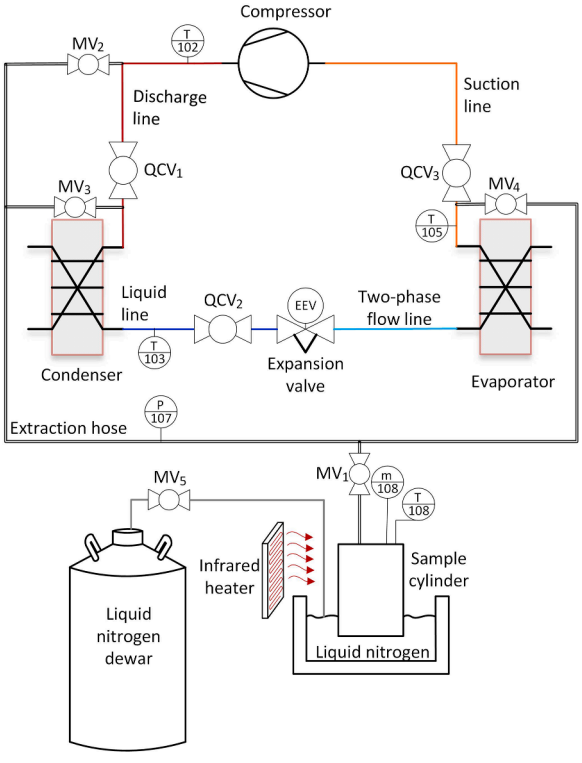

Fig. 2. Refrigerant extraction scheme.

Table 3
Sections of the heat pump.

Section	Measured volume	Calculated volume
1-Compressor+Discharge Line	2.48 dm^3	–
2-Condenser+Liquid Line	0.48 dm^3	0.44 dm^3
3-Evaporator+Electronic expansion valve (EEV)+Two-Phase Line	0.89 dm^3	0.81 dm^3

Table 4
Uncertainty of different measures.

Variable	Systematic uncertainty (95% confidence)	Random uncertainty (95% confidence)	Overall uncertainty
$T_{w,in}$	±0.07 °C	±0.01 °C	±0.07 °C
$T_{w,out}$	±0.07 °C	±0.01 °C	±0.07 °C
$\dot{m}_w$	±0.87 kg h^{-1}	±0.25 kg h^{-1}	±0.90 kg h^{-1}
$\dot{E}_{comp}$	±16.2 W	±0.13 W	±16.2 W
m_{ins}	±1.62 g	±0.83 g	±1.82 g*
m_{ext}	±0.15 g	±0.02 g	±0.15 g
V_{comp}	±0.077 dm^3**	±0.039 dm^3	±0.079 dm^3
V_{cond}	±0.077 dm^3**	±0.016 dm^3	±0.077 dm^3
V_{evap}	±0.077 dm^3**	±0.023 dm^3	±0.078 dm^3
P_{ref}	±1.55 kPa	±0.58 kPa	±1.65 kPa
T_{ref}	±0.8 °C	±0.001 °C	±0.8 °C

* Expanded uncertainty of a single point measure.
** Calculated using error propagation of pressure and temperature used to calculate the volume.

±0.1, respectively. In terms of refrigerant charge, the uncertainty of adding mass extracted and remaining mass in every section are ±0.19 g for compressor section, and ±0.18 g for the condenser and evaporator sections.

2.3. Test campaign

Three different test campaigns have been developed. Table 5 shows details of the tests performed.

The first one, labelled reference, is a test in the nominal working conditions (B0W35 at 60 Hz) with 10 K of SH. Previous charge optimisation tests were made in order to set 195 g as the optimal refrigerant charge.

The second test campaign is labelled SCOP (seasonal coefficient of performance) tests (numbered from test 2 to test 8). They maintain the same refrigerant charge used in the nominal point. Secondary fluid conditions are set according to the standard EN14825 (European Committee for Standardization, 2019b) for determining seasonal COP. In the case of this brine-to-water heat pump, tests at different partial loads mean a change in compressor speed (from 20 Hz to 120 Hz) and a variation in the water temperature sent to the building. These tests are labelled as SCOP A to SCOP E. Two additional tests were planned in order to cover all the range with additional compressor speeds and corresponding water outlet temperature. These tests are labelled as Extra SCOP 1 and Extra SCOP 2 (tests number 4 and 6)

The third test campaign is focused on parameter variation over the nominal point. Tests performed in this third campaign are:

-Overcharged test, which aims to know performance variation and the location of the excess of charge.
-Superheat (Sh) variations of 5 and 15 K (test number 10 and 11), where the objective is to test the influence of superheat in performance and charge distribution.
-A special test where a heating wire heats the compressor crankcase (test number 12). The objective is to investigate the effect of the oil temperature on charge distribution.
-Test varying source and side water/brine temperatures (tests number 13 – 15). The objective is to analyse the influence of external temperatures on the charge distribution, mainly in the heat exchangers.

Each test of this 3rd campaign uses an optimised charge amount that gives the best COP values at the specific test condition. This charge was obtained with previous tests dedicated to this purpose.

All tests performed maintain a brine/water temperature difference of 3 K on the source side and 5 K on the sink side.

3. Results and discussion

The results obtained will be explained divided into two groups separately, performance results and refrigerant distribution results. Before performance results, the charge characterisation of the nominal point is shown to take the decision of the nominal charge of the unit. This type of test was repeated to know the refrigerant charge of every test of the “Parameters Variation” campaign, using the same criterion, to maximise COP.

3.1. Charge determination

These results were recorded after adding 10 g of refrigerant in each

Table 5
Test conditions.

Test	Campaign type	Test name	Condition	*n* (rps)	Sh (K)	RefrigerantNominal charge (g)
1	Reference	Nominal	B0W35	60	10	195
2	SCOP	SCOP E	B0W35	120	10	195
3		SCOP A	B0W34	104	10	195
4		Extra SCOP 1	B0W32	90	10	195
5		SCOP B	B0W30	74	10	195
6		Extra SCOP 2	B0W29	60	10	195
7		SCOP C	B0W27	40	10	195
8		SCOP D	B0W24	20	10	195
9	Parameters Variation	Overcharged	B0W35	60	10	254
10		SH5	B0W35	60	5	220
11		SH15	B0W35	60	15	160
12		Comp. heated	B0W35	60	10	180
13		Source var 1	B7W35	60	10	195
14		Source var 2	B13W35	60	10	195
15		Sink var	B0W55	60	10	195

step and waiting to reach steady state (defined as 15 min with measured variables under thresholds imposed by the characterisation standard).

The trend in all the series is similar. Heating Capacity and COP start with a sharp increase until they stabilise in a flat region. Heating capacity is still growing in some tests (B13W35, B0W55 and the peak-valley variation observed in test SH5), but COP declines softly from the maximum.

As seen in Fig. 3 the optimum charge established is 195 g for nominal point, B0W55, B7W35 and B13W35. 180 g is determined as the optimum point for Compressor Heated case, 160 g is the optimum observed for SH15 case, and 220 g is the optimum charge determined for SH5 test.

3.2. Performance results analysis

Table 6 shows the results of the tests in terms of performance. Performance tests campaign determines the declared capacity of the unit and the SCOP. For brine-to-water heat pumps, partial load conditions are determined with different compressor speeds maintaining conditions on the source side and adapting the water supply on the sink side as determined by the European standard (European Committee for Standardization, 2019b). The unit has a declared capacity of $\dot{Q}_h = 9.49\ kW$ (without considering auxiliary electrical support) at full load (120 rps of compressor speed). Charge specific heating capacity of this unit is $C_c = 48.72\ kW\ kg^{-1}$. This result shows that with the current refrigerant charge limit of 150*g*, it is possible to obtain a heating capacity of $\dot{Q}_h = 7.31\ kW$. From the performance tests can be obtained the SCOP for average climates obtaining a value of $SCOP = 4.01$.

Fig. 4 shows the variation of heating capacity and COP for the different points of the Performance test campaign depending on the compressor speed.

Heating capacity shows a linear variation with compressor speed from a minimum value of $\dot{Q}_h = 1.56\ kW$ at $n = 20\ rps$ to the maximum value of $\dot{Q}_h = 9.49\ kW$ at $n = 120\ rps$. This is explained as the volumetric efficiency doesn't vary significantly, and the suction density remains practically constant in all tests.

COP also shows a quasi-linear variation (opposite to the heating capacity) with the minimum $COP = 3.21$ at $n = 120\ rps$ and maximum $COP = 4.89$ at $n = 20\ rps$. As the compressor speed increases, the isentropic and total efficiencies of the compressor decrease, making the global efficiency decrease as well.

Fig. 5 shows the subcooling (SC) and approach temperatures measured in the condenser and evaporator in each test.

Approach temperatures in the condenser and evaporator are defined as:

$$\delta T_{cond} = T_{cond,out} - T_{w,in} \tag{9}$$

$$\delta T_{evap} = T_{b,in} - T_{evap,out} \tag{10}$$

These variables give us knowledge about the heat exchangers' size compared with their thermal capacity.

Fig. 5 shows that minimum subcooling is obtained at the minimum compressor speed, raising its value at higher compressor speeds. No linear dependence with compressor speed is detected, and subcooling values at higher compressor speeds are between $Sc = 3.76\ K$ and $Sc = 5.13\ K$.

Approach temperature in the evaporator is less than 1 K for all points except $n = 120\ rps$ showing that the evaporator area is enough for the capacity needed (even a little oversized) except in the case of maximum speed where the approach is $T_{evap} = 3.32\ K$.

The approach temperature in the condenser is quite variable, showing its minimum at 74 Hz (impossible negative values are due to measurement uncertainties). Maximum values of $\delta T_{cond} = 3.14\ K$ are obtained. These results show that the condenser is a little bit undersized at some compressor speeds, having the opportunity to obtain higher performance increasing the area but with the counterpart of increasing refrigerant charge.

3.3. Refrigerant charge distribution

Table 7 shows refrigerant inserted in each test and the charge determined in each heat pump section, including the pneumatic valves.

Fig. 6 shows charge results for the nominal point. Charge in liquid, suction and discharge line are calculated based on the density measured and subtracted from the corresponding sections in order to determine the charge in the compressor, condenser and evaporator. Charge specific capacity for this nominal point is $C_c = 23.08\ kW\ kg^{-1}$.

41.5% of the refrigerant charge is stored in the compressor. This high value can only be explained by the refrigerant trapped dissolved in the oil. The next component storing charge is the evaporator with 27.8% of the charge and then the condenser with 23.9%. The remaining charge is mainly located in the liquid line with 4.5% and pneumatic valves with 1.5%. Gas lines (suction and discharge) account for 0.8%.

Compressor results are explained due to refrigerant solubility in the compressor oil. The oil volume for this compressor model is 0.4 l (0.4 kg), and refrigerant mass solubilities of 10% or even more are typical.

In the literature, it is generally found that the condenser is the component that requires the most amount of refrigerant charge, reaching values of more than the half refrigerant charge (Chen et al., 2019; Li et al., 2015). In these references, the condenser volume is considerably higher than other components, and the subcooling value is also higher. In this case, as the refrigerant charge selected is the one that optimises the COP, it is reached with a low level of SC (around 3 K). Therefore, the condenser has a similar refrigerant charge to the evaporator, instead of a considerably higher value. The reason for the higher charge stored in the evaporator than in the condenser, although there are lower refrigerant qualities and densities, is not straightforward. Liquid refrigerant stored in the inlet distributor or maldistribution problems can be the reasons for this performance.

Fig. 7 shows the charge variation in the SCOP campaign for the compressor, the evaporator and the condenser section. The refrigerant charge stored in the lines and the pneumatic valves is not plotted as the

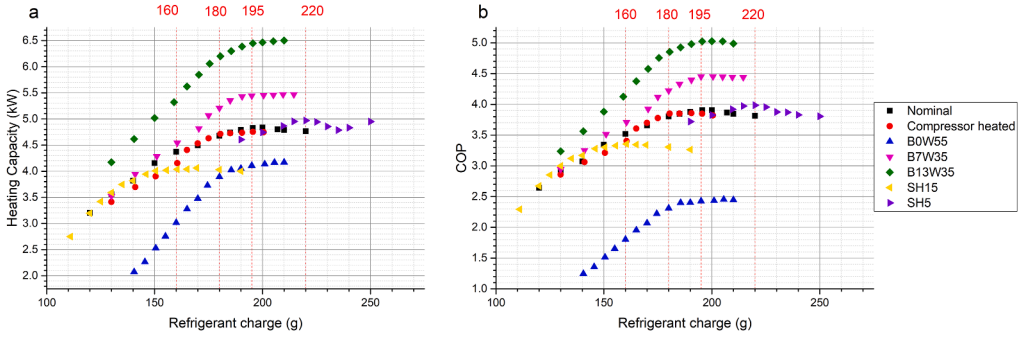

Fig. 3. Optimal COP determination.

Table 6
Performance results of the test.

		Condition	$\dot{Q}_h$ (kW)	COP (-)	n (Hz)	P_{dis} (bar)	P_{suc} (bar)	T_{cond} (°C)	T_{evap} (°C)	T_{dis} (°C)	T_{oil} (°C)	Sc (K)	Sh (K)
	1	B0W35	4.5 ± 0.1	3.7 ± 0.1	60	11.8	3.6	33.7	−9.0	62.5	48.8	0.7	10
SCOP	2	B0W35	9.5 ± 0.1	3.2 ± 0.1	120	12.3	3.2	35.4	−12.2	72.3	55.9	3.8	10
	3	B0W34	8.7 ± 0.1	3.4 ± 0.1	108	12.2	3.4	34.9	−10.6	70.0	50.1	5.1	10
	4	B0W32	7.3 ± 0.1	3.8 ± 0.1	90	11.5	3.5	32.6	−10.1	63.8	52.6	4.0	10
	5	B0W30	5.7 ± 0.1	3.9 ± 0.1	74	10.9	3.5	30.4	−9.9	60.9	44.8	4.6	10
	6	B0W29	4.8 ± 0.1	4.3 ± 0.1	60	10.4	3.5	28.6	−9.6	55.2	45.2	3.6	10
	7	B0W27	3.3 ± 0.0	4.8 ± 0.2	40	9.8	3.8	26.2	−7.0	47.5	37.3	1.3	10
	8	B0W24	1.6 ± 0.0	4.9 ± 0.5	20	9.2	3.8	23.6	−7.5	45.5	36.3	0.1	10
Parameter Variation	9	Overfilled	4.7 ± 0.1	3.7 ± 0.1	60	12.4	3.6	35.6	−9.1	64.8	48.4	7.7	10
	10	SH5	4.9 ± 0.1	4.0 ± 0.1	60	12.1	3.8	34.6	−6.8	56.4	48.2	0.9	5
	11	SH15	4.0 ± 0.1	3.3 ± 0.1	60	11.9	3.0	34.1	−14.0	70.6	58.2	2.1	15
	12	Comp H*	4.7 ± 0.1	3.8 ± 0.1	60	12.0	3.5	34.3	−9.6	66.9	65.3	3.1	10
	13	B7W35	5.4 ± 0.1	4.4 ± 0.1	60	12.1	4.3	34.6	−3.2	59.8	50.6	0.7	10
	14	B15W35	6.1 ± 0.1	5.0 ± 0.2	60	12.1	5.1	34.7	2.6	56.8	49.1	0.0	10
	15	B0W55	4.2 ± 0.1	2.5 ± 0.1	60	18.5	3.5	53.6	−9.4	90.8	78.1	2.7	10

* COP calculated without considering the heating wire electrical consumption. Considering it, the COP is 3.41.

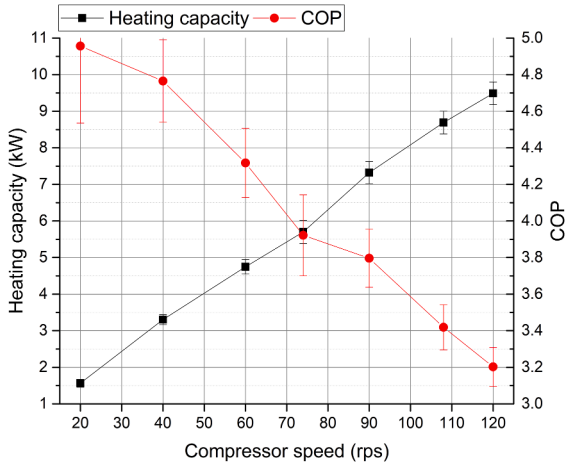

Fig. 4. Heating capacity and COP variation.

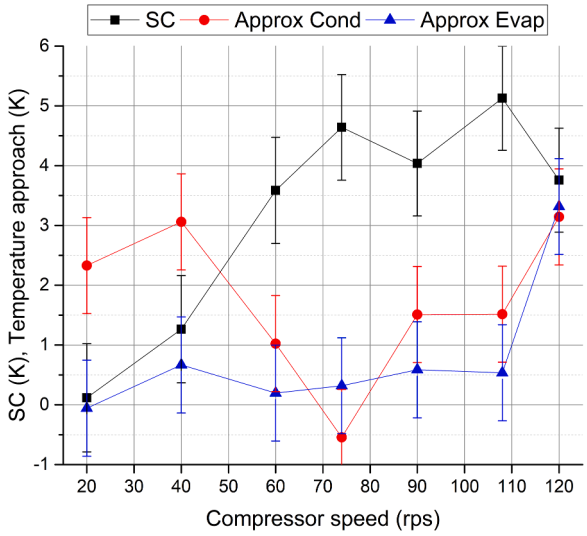

Fig. 5. SC and temperature approach in heat exchangers.

values are approximately constant over the test campaign.

A first observation is that compressor speed variation from 20 rps to 120 rps does not make big differences in charge stored in the different elements of the unit.

No clear relationship between compressor speed and oil solubility (shown in terms of the charge stored in the compressor) is reported. From the maximum speed to the minimum, oil temperature decreases and discharge pressure (see Table 6), compensating each other for the oil solubility values and having a small variation of the charge stored in the compressor. It seems that discharge pressure has more effect than compressor oil temperature in solubility values if we observe the variations between tests 1 and 6 working at the same compressor speed but at different sink side temperatures. Although oil temperature is lower in test 6 (from 48.8 °C to 45.2 °C), pushing for increasing oil solubility; discharge pressure is also lower (from 11.81 bar to 10.42 bar), having the opposite effect, and the net result is a decrease in oil solubility giving lower charge stored in the compressor from Test 6 (75.6 g) to Test 1 (83.6 g)

These small charge variations in the compressor explain the differences in the condenser and evaporator (as the total charge remains constant). Charge differences are stored in the condenser, in the liquid section, increasing or decreasing the subcooling, but there is no linear relation between *Sc* and charge stored in the condenser. Tests with low refrigerant charge in the condenser have low subcooling, but there is no correlation in the tests with SC between 3 and 5 K. In the evaporator, different mass flow rates change the refrigerant distribution between channels and their internal void fraction.

In the second test campaign, Fig. 8, the variations in refrigerant charge amount are more significant. Test 2 (SCOP E) was added to this figure because the only difference with the nominal point is the compressor speed.

In this campaign, except for more compressor speed and overfilled tests, the tests are done with the optimum refrigerant charge. Charge specific capacity varies from the nominal point (23.08 $kW\,kg^{-1}$) to the minimum value obtained in the overfilled test (18.43 $kW\,kg^{-1}$) and to the maximum value obtained in the test SCOP E (48.72 $kW\,kg^{-1}$)

Regarding the results, there is a slight decrement in refrigerant charge in the compressor and evaporator when increasing the compressor speed without changing any of the other conditions. The decrement in suction pressure can explain the effect on the evaporator. Charge reduction in the compressor with increasing compressor speed is explained by the rise of oil temperature maintaining similar discharge pressures (signal of an oversized condenser).

The following comparison is test 1 (nominal) and test 9 (overfilled), where the only difference is the refrigerant charge amount. In this comparison, 60 g of propane were added, expecting to be stored in the condenser, increasing the subcooling and discharge pressure. As expected, almost all the refrigerant amount went to the condenser, which increased the subcooling level to 7 K, increasing the discharge pressure. However, approximately 10 out of 60 g of propane went to the evaporator instead of the condenser. It is caused because the condenser could

Table 7
Refrigerant charge distribution in the heat pump.

	Test	Condition	Refrigerant inserted (g)	Section compressor (g)	Section condenser (g)	Section evaporator (g)	Pneumatic valves (g)
	1	B0W35	195.5 ± 1.82	83.6 ± 0.19	51.6 ± 0.18	56.9 ± 0.18	3.3 ± 0.15
SCOP	2	B0W35	196 ± 1.82	81.1 ± 0.19	57 ± 0.18	54.7 ± 0.18	3.0 ± 0.15
	3	B0W34	195 ± 1.82	75.6 ± 0.19	57.1 ± 0.18	58.2 ± 0.18	3.5 ± 0.15
	4	B0W32	198 ± 1.82	71.4 ± 0.19	61.3 ± 0.18	62 ± 0.18	3.7 ± 0.15
	5	B0W30	195.5 ± 1.82	75.4 ± 0.19	63.4 ± 0.18	52.6 ± 0.18	3.0 ± 0.15
	6	B0W29	195.5 ± 1.82	75.6 ± 0.19	60 ± 0.18	56.3 ± 0.18	3.7 ± 0.15
	7	B0W27	195.0 ± 1.82	74.3 ± 0.19	54.4 ± 0.18	61.6 ± 0.18	3.0 ± 0.15
	8	B0W24	195.0 ± 1.82	75.4 ± 0.19	52.6 ± 0.18	62.1 ± 0.18	3.3 ± 0.15
Parameter variation	9	Overfilled	254.0 ± 1.82	84.4 ± 0.19	103.2 ± 0.18	63.2 ± 0.18	3.6 ± 0.15
	10	SH5	220.0 ± 1.82	87.5 ± 0.19	52.8 ± 0.18	76.7 ± 0.18	4.2 ± 0.15
	11	SH15	160.0 ± 1.82	62.7 ± 0.19	56.9 ± 0.18	39.3 ± 0.18	2.7 ± 0.15
	12	Com	190.0 ± 1.82	72.5 ± 0.19	60.1 ± 0.18	52.9 ± 0.18	1.6 ± 0.15
	13	B7W35	195.0 ± 1.82	88.6 ± 0.19	51.1 ± 0.18	51.9 ± 0.18	3.2 ± 0.15
	14	B15W35	196.0 ± 1.82	95.4 ± 0.19	49.2 ± 0.18	51.9 ± 0.18	1.6 ± 0.15
	15	B0W55	196.0 ± 1.82	89.1 ± 0.19	60.5 ± 0.18	46.7 ± 0.18	3.3 ± 0.15

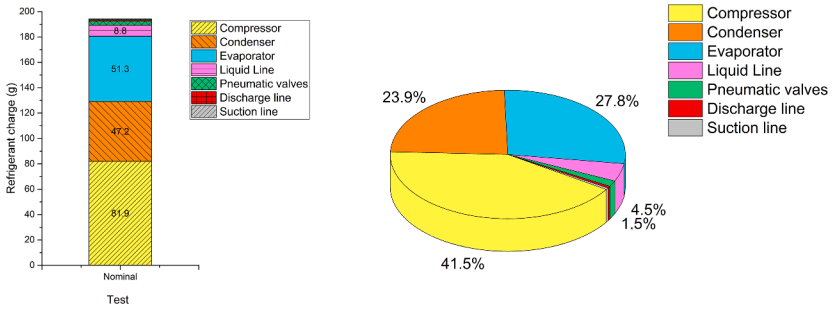

Fig. 6. Results of refrigerant charge distribution in the nominal point.

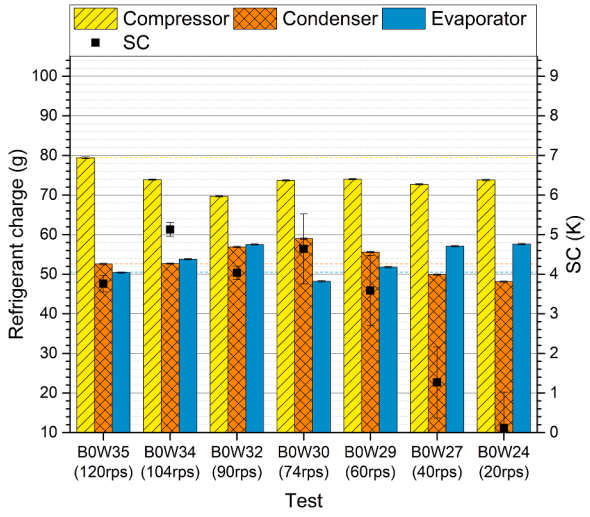

Fig. 7. Refrigerant distribution results of the SCOP campaign.

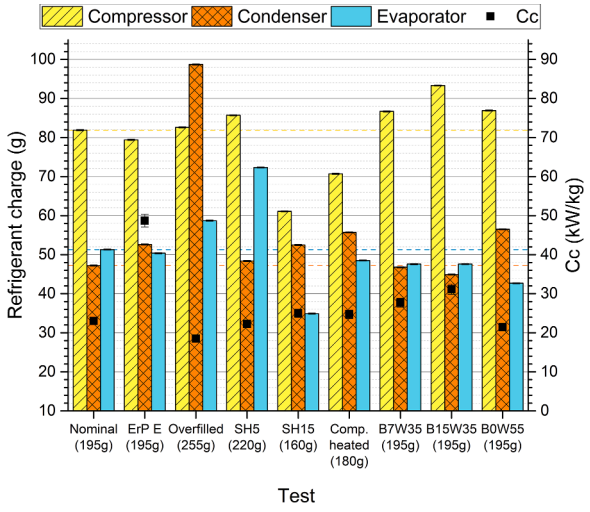

Fig. 8. Refrigerant distribution results of the singular variations campaign.

still increase the subcooling level without increasing discharge pressure, reducing the approximation in the condenser and the quality inlet in the evaporator.

The subsequent study is the superheat's impact, tests 10 (SH5) and 11(SH15). In this case, the tests show that the evaporator is oversized too; therefore, the evaporation pressure is linked with the superheat level. When the superheat is reduced, the evaporation temperature increases, and the part of the evaporator occupied by the refrigerant in the gas state is reduced. Consequently, the evaporator has more volume occupied by the refrigerant in two-phase flow at a higher pressure than the reference case. All this led to an increase in refrigerant charge in the evaporator. In the compressor, the oil temperature is lower, increasing the solubility and the refrigerant amount in this component. The condenser, by contrast, is not affected by the superheat. On the other hand, in the case of increasing the superheat (test 11, SH15), the effect observed is the opposite; there is a refrigerant amount reduction in the compressor and the evaporator because of the reasons already mentioned.

The fourth study was the compressor heated with the heating wire (test 12, Comp. Heated). In this case, the solubility is reduced because of the increase in oil temperature, and the total amount of refrigerant in the compressor drops. Nevertheless, in the heat exchangers, there is no effect.

Then, in the source temperature variation tests from 0 °C to 7 °C and

15 °C (test B7W35 and test B15W35), there is an increase in the compressor refrigerant charge, maintaining similar charge values in the condenser and evaporator.

Lastly, in the sink temperature variation tests from 35 °C to 55 °C (test 15, B0W55), a slight increase in the charge stored in the compressor and condenser is observed, and a reduction in the evaporator. Changes in the evaporator can be explained due to the higher quality at the evaporator inlet, reducing the liquid stored.

As seen in the results of the singular variations, three effects impact the refrigerant charge in the components. In the compressor, the refrigerant inside the oil has the most influence on the total refrigerant in this component. To reduce the refrigerant in the oil, the oil's temperature should be increased, working pressure should be decreased, or the lubricant amount should be decreased. Usually, the operating pressure is marked by the secondary fluid and the condenser's size. The manufacturer sets the amount of oil, but reductions may be performed in the design process. Lastly, in this case, the oil temperature increment has been done with a heating wire, but it is necessary to find other option that does not impact the COP.

In the evaporator, superheating affects the volume percentage used by the gas phase. Therefore, higher superheats determine lower charge stored in the evaporator.

Additionally, the quality of the evaporator's inlet considerably affects the amount in this component.

Comparing the two tests that have reduced the amount of charge needed, increasing the oil temperature with a heating wire meant a reduction of the COP of approximately 0.45, which only meant a decrease of 5 g. However, increasing the superheat up to 15 K meant a reduction of COP of about 0.5 in the nominal conditions, but the reduction in refrigerant charge was 35 g. Still, with the increase of superheat, the heating capacity was reduced because of the density reduction at the compressor suction.

4. Conclusions

The current study presents experimental performance and refrigerant distribution in different test conditions in a low-charge brine-to-water heat pump built with commercially available components.

The unit has a declared heating capacity of $\dot{Q}_h = 9.5\ kW$ using a charge of $m = 195\ g$ of propane with a charge specific capacity of $C_c = 48.72\ kW\ kg^{-1}$.

The compressor requires almost half of the refrigerant charge at the nominal point (41.5%). The rest of the refrigerant is located in the heat exchangers almost evenly, with the evaporator 27.8% and the condenser 23.9%. The refrigerant charge stored in the lines is negligible compared with the other components mentioned.

In the partial load test campaigns, following the standard 14,825, there are no big charge percentage variations. This campaign makes the heat pump work at different compressor speeds and different sink temperatures.

A general conclusion of the SCOP campaign is that further charge reduction in these units has to be focused on the charge stored in the oil (reducing solubility or oil quantity), reducing the evaporator volume and understanding the complex phenomena of maldistribution.

With the singular variation campaign it can be extracted several conclusions:

- Compressor speed variation has no effect on charge distribution for this unit.
- Superheat control affects in a great way the refrigerant charge stored in the evaporator and the compressor due to the variation in evaporation pressure and compressor oil temperature. A compromise in the superheat value is needed as higher values demand lower charge, but COP is degraded.
- Variations of source-side temperatures mainly affect the refrigerant charge stored in the compressor, while sink-side temperatures mainly affect the refrigerant charge stored in the evaporator.

Results obtained can state that with current commercially available components, it is possible to build a brine-to-water heat pump with a capacity of 7.3 kW using a refrigerant charge of 150 g of propane.

It can be used the SH level or a heating wire to reduce the refrigerant charge needed in the compressor, but it reduces the overall COP. It would mean a very effective refrigerant charge reduction strategy if a different way of heating the oil without losing performance can be found.

Declaration of Competing Interest

The authors declare that they have no known competing financial interests or personal relationships that could have appeared to influence the work reported in this paper.

Acknowledgements

The authors would like to acknowledge the Spanish "MINISTERIO DE CIENCIA E INNOVACIÓN", through the project ref-PID2020–115665RB-I00 "Descarbonización de Edificios e Industrias con sistemas híbridos de bomba de Calor" for the given support.

The authors also would like to acknowledge the "Consellería dInnovació, Universitats, Ciencia i Societat Digital de la Generalitat Valenciana" through the Project "AICO/2021/078" for the given support.

Also, the study presented in this paper received funding from the German Federal Ministry of Economic Affairs and Climate Action (BMWK) under the grant agreement numbers FKZ 03EN4001A (LC150).

Lastly, the experimental campaign was performed during an international stay financed by "Ayudas para movilidad de estudiantes de Doctorado de la Universitat Politècnca de València" during the doctoral thesis financed by (PAID-01–17)

References

Andersson, K., Granryd, E., Palm, B., 2018. Water to water heat pump with minimum charge of propane. Refrigeration Science and Technology. International Institute of Refrigeration, pp. 725–732. https://doi.org/10.18462/iir.gl.2018.1264.

Chen, R., Wu, J., Duan, J., 2019. Performance and refrigerant mass distribution of a R290 split air conditioner with different lubricating oils. Appl. Therm. Eng. 162, 114225 https://doi.org/10.1016/j.applthermaleng.2019.114225.

Clodic, D., Palandre, L., 2002. Refrigerant capacity ratio as an indicator to evaluate advance technology for low charge refrigerant systems. Zero Leakage–Minimum Charge. IIF–IIR, Stockholm, Suede.

Coleman, H.W., Steele, W.Glenn., Coleman, H.W., 2009. Experimentation, Validation, and Uncertainty Analysis for Engineers. John Wiley & Sons.

Corberán, J.M., Martínez, I.O., Gonzálvez, J., 2008. Charge optimisation study of a reversible water-to-water propane heat pump. Int. J. Refrig. 31, 716–726. https://doi.org/10.1016/j.ijrefrig.2007.12.011.

Domanski, P.A., Brignoli, R., Brown, J.S., Kazakov, A.F., McLinden, M.O., 2017. Frigorigènes à faible GWP pour les applications à moyenne et haute pression. Int. J. Refrig. 84, 198–209. https://doi.org/10.1016/j.ijrefrig.2017.08.019.

Energy consumption in households - Statistics Explained [WWW Document], 2021. URL https://ec.europa.eu/eurostat/statistics-explained/index.php?title=Energy_consumption_in_households#Energy_products_used_in_the_residential_sector (accessed 7.28.21).

European Commission, 2019. The European Green Deal. Brussels.

European Committee for Standardization, 2019a. EN 14511-3 air conditioners, liquid chilling packages and heat pumps for space heating and cooling and process chillers, with electrically driven compressors - part 3: test methods.

European Committee for Standardization, 2019b. EN 14825 - air conditioners, liquid chilling packages and heat pumps, with electrically driven compressors, for space heating and cooling - testing and rating at part load conditions and calculation of seasonal performance.

European Committee for Standardization, 2016. EN 378-1:2016 refrigerating systems and heat pumps - safety and environmental requirements - part 1: basic requirements, definitions, classification and selection criteria.

Fernando, P., Palm, B., Lundqvist, P., Granryd, E., 2004. Propane heat pump with low refrigerant charge: design and laboratory tests. Int. J. Refrig. 27, 761–773. https://doi.org/10.1016/J.IJREFRIG.2004.06.012.

Hrnjak, P., Litch, A.D., 2008. Microchannel heat exchangers for charge minimization in air-cooled ammonia condensers and chillers. Int. J. Refrig. 31, 658–668. https://doi.org/10.1016/J.IJREFRIG.2007.12.012.

Hrnjak, P.S., Hoehne, M.R., 2004. Charge minimization in systems and components using hydrocarbons as a refrigerant. ACRC TR-224 61801.

IEC, I.E.C., 2022. IEC 60751:2022 industrial platinum resistance thermometers and platinum temperature sensors. Int. Standard.

International Organization for Standardization (ISO), 1995. Guide to the Expression of Uncertainty in Measurement. Geneva.

Joint Committee for Guides in Metrology (JCGM), 2008. Evaluation of Measurement Data-Guide to the Expression of Uncertainty in Measurement.

Kujak, S., Schultz, K., 2016. Insights into the next generation HVAC&R refrigerant future. Sci. Technol. Built Environ. 22, 1226–1237. https://doi.org/10.1080/23744731.2016.1203239.

Lemmon, E.W., Bell, I.H., Huber, M.L., McLinden, M.O., 2018. NIST Standard Reference Database 23: Reference Fluid Thermodynamic and Transport Properties-REFPROP.

Li, H., Hrnjak, P., 2015. An experimentally validated model for microchannel heat exchanger incorporating lubricant effect. Int. J. Refrig. 59, 259–268. https://doi.org/10.1016/J.IJREFRIG.2015.07.020.

Li, T., Lu, J., Chen, L., He, D., Qiu, X., Li, H., Liu, Z., 2015. Measurement of refrigerant mass distribution within a R290 split air conditioner. Int. J. Refrig. 57, 163–172. https://doi.org/10.1016/J.IJREFRIG.2015.05.012.

Lorentzen, G., 1995. The use of natural refrigerants: a complete solution to the CFC/HCFC predicament. Int. J. Refrig. 18, 190–197. https://doi.org/10.1016/0140-7007(94)00001-E.

Lund, J., 2001. Geothermal heat pumps - an overview. Geo-Heat Center Q. Bull. 22, 1–2.

Marvillet, C., 1995. Performances des systèmes frigorifiques : influence des fuites. Rev. Prat. Froid Condition. d'air.

McLinden, M.O., Brown, J.S., Brignoli, R., Kazakov, A.F., Domanski, P.A., 2017. Limited options for low-global-warming-potential refrigerants. Nat. Commun. 8 https://doi.org/10.1038/ncomms14476.

Mulroy, W.J., Didion, D.A., 1985. Refrigerant Migration in a Split-Unit Air Conditioner. ASHRAE Trans.

Peuker, S., 2010. Experimental and analytical investigation of refrigerant and lubricant migration. Springer Proceedings in Physics. University of Illinois at Urbana-Champaign. https://doi.org/10.1007/978-3-319-30602-5_43.

Pitarch, M., Navarro-Peris, E., Gonzálvez-Maciá, J., Corberán, J.M., 2017. Evaluation of different heat pump systems for sanitary hot water production using natural refrigerants. Appl. Energy 190, 911–919. https://doi.org/10.1016/j.apenergy.2016.12.166.

Poggi, F., Macchi-Tejeda, H., Leducq, D., Bontemps, A., 2008. Refrigerant charge in refrigerating systems and strategies of charge reduction. Int. J. Refrig. 31, 353–370. https://doi.org/10.1016/J.IJREFRIG.2007.05.014.

Regulation (EU), 2014. Regulation (EU) No 517/2014 of the European Parliament and of the council of 16 April 2014 on fluorinated greenhouse gases and repealing regulation (EC) No 842/2006. Off. J. Eur. Union, 2014, L150/195-230.

Sieres, J., Ortega, I., Cerdeira, F., Álvarez, E., 2020. Influence of the refrigerant charge in an R407C liquid-to-water heat pump for space heating and domestic hot water production. Int. J. Refrig. 110, 28–37. https://doi.org/10.1016/j.ijrefrig.2019.10.021.

Xu, B., Wang, Y., Chen, J., Li, F., Li, D., Pan, X., 2016. Investigation of domestic air conditioner with a novel low charge microchannel condenser suitable for hydrocarbon refrigerant. Measurement (Lond) 90, 338–348. https://doi.org/10.1016/j.measurement.2016.04.034.